Journal of African Earth Sciences 178 (2021) 104182

Contents lists available at ScienceDirect

Journal of African Earth Sciences

journal homepage: www.elsevier.com/locate/jafrearsci

Talc schist deposits from central Cameroon: Mineralogical and physico-chemical characterization

D.L. Woguia [a,*], N. Fagel [a], E. Pirard [b], A. Gourfi [c], L.M. Ngo bidjeck [d], M. El ouahabi [a]

[a] UR. Clay, Geochemistry and Sedimentary Environments (AGEs), Department of Geology, Faculty of Sciences, University of Liège, Liége, B-4000, Belgium
[b] Faculty of Applied Sciences, B.52, Sart- Tilman, University of Liège, B-4000, Belgium
[c] Department of Geology, Faculty of Applied Sciences, University of Cadi Ayyad, Marrakech, Morocco
[d] Department of Geology, University of Yaoundé1, Cameroon

ARTICLE INFO

Keywords:
Talc schist
Mineralogy
Clay
Geochemistry
Cameroon

ABSTRACT

Talc schist deposits are reported in central Cameroon region, and different alteration zones were determined depending on differences related to the texture and color of the host rock. For the purpose of determining mineralogical and physicochemical characteristics of talc schist, a total of 45 samples from the sites studied were collected and analyzed using an array of physico-chemical methods.

Talc schist samples are mainly composed of variable amount of talc associated with plagioclase and clay minerals. Three groups of mineral association were determined: i) talc with small amount of chlorite and traces of kaolinite, ii) talc with high amount of chlorite, iii) variable amount of talc with plagioclase and clay minerals. The talc schist samples have homogeneous grain-sizes and are classified as silty sand or sandy silt.

The occurrence of Ni and Cr in the talc schists are consistent with the composition of the talc deposits formed in relation to ultramafic rocks. The genesis of talc is due to hydrothermal fluid circulation in ultramafic rocks, attested by the occurrence of S and P.

1. Introduction

Talc is widely used in various industrial applications because of its particular physico-chemical properties, such as high thermal stability, low electrical conductivity, good absorption and desorption properties, wide particle-size distribution, and large specific surface area (Nkoumbou et al., 2007; Dumas et al., 2013; Ersoy et al., 2013). Chemical composition of talc is mainly related to the nature of the protolith and the physicochemical conditions that preceded its formation.

Unlike synthetic talc, natural talc occurs in association with other mineral phases such as calcite, dolomite, magnesite, asbestiform and non-asbestiform minerals, tremolite, anthophyllite, quartz, pyrophyllite, micas, chlorite, antigorite and much more rarely chrysotile and lizardite (Marteau et al., 1991). The associated minerals will depend on the type and the nature of the transformation that has occurred in the parent rock.

Talc typically forms from hydrothermal alteration or metamorphism of dolomites and ultrabasic rocks (Evans and Guggenheim, 1988; Schandl et al., 2002; Ali-Bik et al., 2012; Gil et al., 2020), but is rarely reported as a sedimentary mineral (Tosca et al., 2011).

Globally, significant talc deposits are rare and only occur in a dozen countries such as China, India, Brazil, the United States, South Korea, France, Japan, Finland and Canada (Marteau et al., 1991).

In Africa, talc deposits occur in Rwanda in the Kibanda site in relation to the regional metamorphic evolution of metasediments and volcanics of the Kibara Supergroup (Prochaska et al., 1992). Talc deposits covered with tropical residual soils occur in southwestern Nigeria (Akpanika et al., 1987).

The first deposits of talc reported in Cameroon are situated in the Northern East of the country in the Bayara and Ngambè localities (Fig. 1) (Laplaine, 1969). Recently, talc schist deposits have been discovered in the locality of Boumnyebel (Nkoumbou et al., 2006a) and its surroundings (Ntep et al., 2001) and the physicochemical properties of talc deposits have been characterized (Nkoumbou et al., 2008a; Yonta et al., 2010) (Fig. 2).

The Boumnyebel deposit has been characterized macroscopically and microscopically with the aim to determine physicochemical properties of talc (Nkoumbou et al., 2008a; Yonta et al., 2010). According to the authors, based on the high talc content of the rocks and occasional coexisting tremolite and magnesio-riebeckite, the origin of the talc

* Corresponding author.
E-mail address: damarislaure.woguia@doct.ulg.ac.be (D.L. Woguia).

https://doi.org/10.1016/j.jafrearsci.2021.104182
Received 5 October 2020; Received in revised form 10 February 2021; Accepted 8 March 2021
Available online 12 March 2021
1464-343X/© 2021 Elsevier Ltd. All rights reserved.

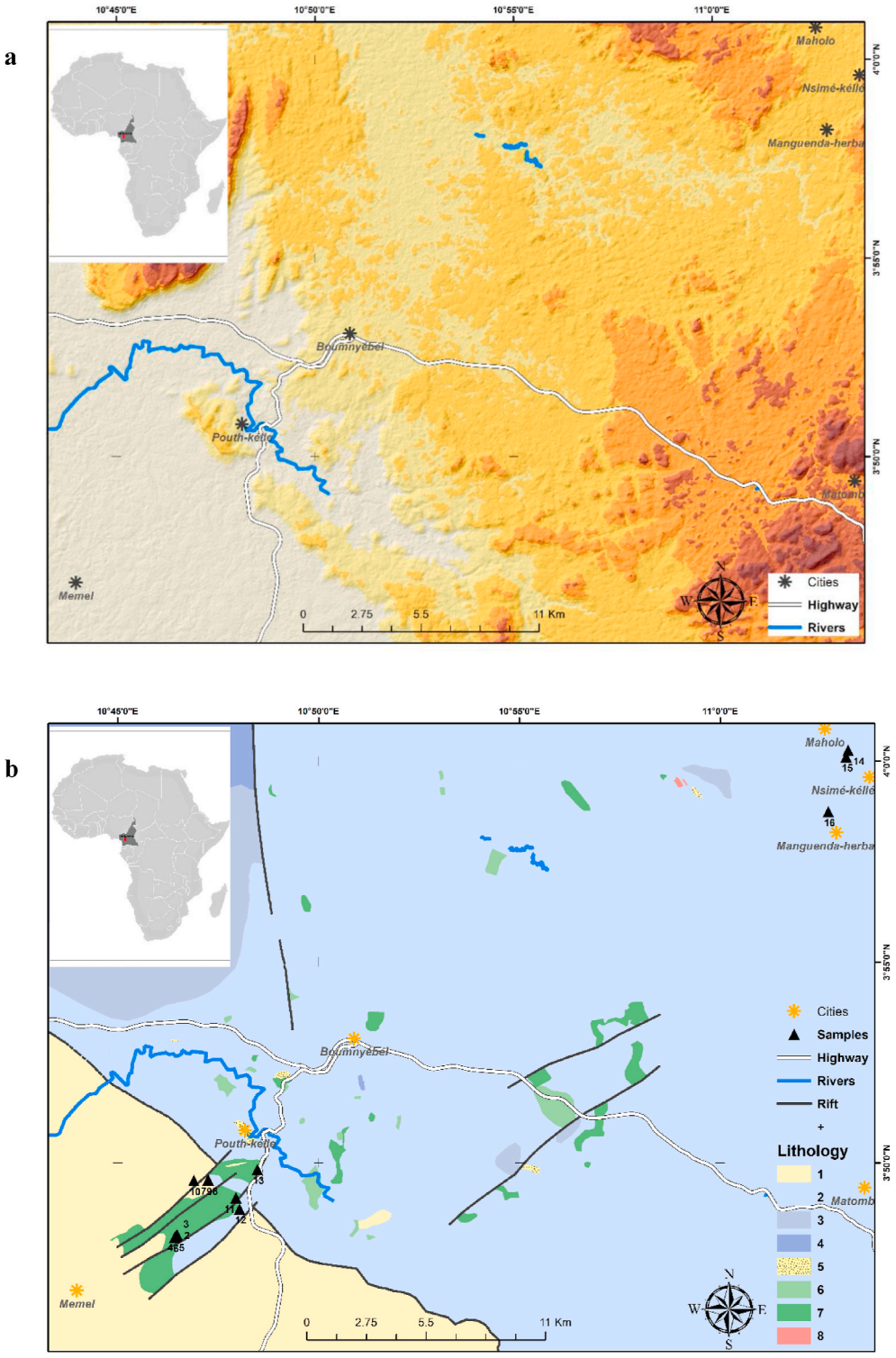

Fig. 1. Geological map and samples location of the studied area. 1. Orthogneiss and associates rocks. 2. Micaschists (biotite-muscovite-garnet). 3. Micaschists (biotite-muscovite-garnet-kyanite). 4. Migmatites. 5. Dolomitic marble and associated talcschists. 6. Metagabrro. 7. Talcschists and associated rocks. 8. Metagabbro.

sediment is assigned to a hydrothermal alteration of ultramafic rocks.

The preliminary results obtained need to be supplemented by more detailed results to understand the genesis of talc sediments, their purities and their distribution on the Cameroon territory. Our study will provide detailed information about talc schist characteristics in several localities in Cameroon, with particular emphasis on spatial variability and the origin of talc schists.

2. Geological setting

The geology of Cameroon is formed by two different domains; the cratonic area comprising the northern edge of the Congo craton which is made up of Archaean and Paleoproterozoic formations and the Pan-African chain of Central Africa (Davison and Dos Santos, 1989; Nzenti et al., 1988; Pouclet et al., 2006). The Pan-African covers two-thirds of the territory of the Yaoundé Group, where talc schist deposits have been

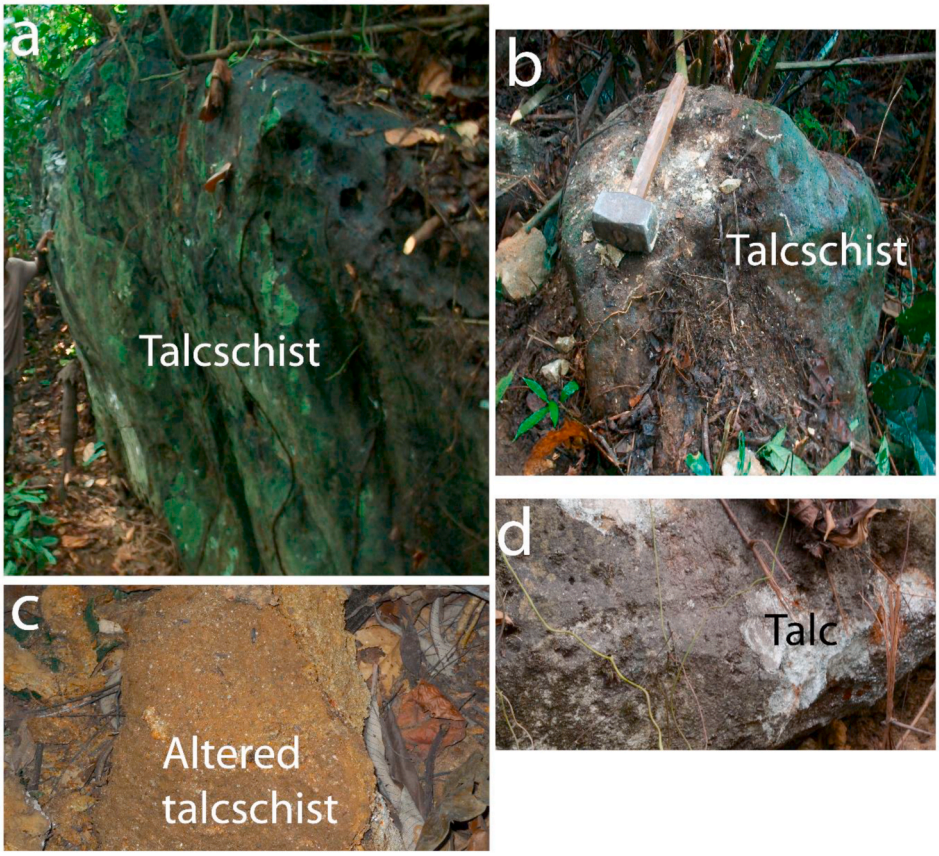

Fig. 2. Lithology and appearances of samples. A. talc schist of Pouth – kélle site; b. talcshist at Mémel site; c. Altered talc schist at Maholo; d. Talc at Pouth-kélle.

found in Cameroon (Fig. 1).

The Yaoundé Group comprises the medium-to high-grade Yaoundé series (Nzenti et al., 1988) and the low-grade Mbalmayo-Ayos-Bengbis series (Nédélec et al., 1986) thrust onto both the Archaean series. The Yaoundé series are formed by sedimentary and igneous rocks recrystallized under medium-to high-temperature metamorphic conditions at high pressure during the Pan-African orogeny (Nzenti et al., 1988; Owona et al., 2011; Stendal et al., 2006; Yonta-Ngouné et al., 2010). The high-grade Yaoundé gneisses includes dolomite-rocks and evaporitic beds sedimented in an intracontinental environment (Nzenti et al., 1988).

Heterogeneous deposits of talc schists occur in the Yaoundé Group, this study will focus on the Mémel, Pouth – Kellé, Nsime – Kélle, Maholè and Manguenda –Hegba area. According to Nkoumbou et al. (2008b), the localities of Mémel and Pouth - Kéllé are located on the border of the Pan - African chain (600 Ma) of the Yaoundé Group and on the North western edge of the Congo craton. Mica schist deposits studied by Nkoumbou et al. (2006a), are associated with hornblendites and chlorite in the locality of Mémel. While, in Pouth - Kélle talcschists are essentially associated with hornblendites having high crystallinity and plasticity. Yonta et al. (2010) show that these rocks form discontinuous levels (≤30 m) in the Pan-African groundwater chain, consisting of muscovite, amphiboles and pyroxenites, and upwards of muscovite locally associated with marbles and amphiboles. Two exceptions have been noted; talc schist is associated with dolomitic marbles at the Henguegue level, and is in contact with the Paleoproterozoic orthogneisses in the Mémel area. Recently, Ngally et al. (2014) studied the possible use of this talc schist for cement aggregates, due to the occurrence of a high amount of magnesium that reacts with phosphate to give cementitious materials such as magnesium phosphate cements.

3. Material and methods

3.1. Material

Sampling was made in the localities arround Boumnyebel during a fieldwork in 2016. The sample locations were based on previous works (Nkoumbou et al., 2006a; Yonta, 2010; Metang 2014) (Fig. 1a). The field survey revealed heterogeneity and change in the facies within the localities studied (Table 1 and Fig. 1b). A total of forty five samples were collected based on the observed macroscopic changes in the talc schist facies (Table 1). Four zones have been sampled.

Thirty five samples were taken in the locality of Mémel site situated South of Boumnyebel (Fig. 1). Most of the samples are grey or yellow. Six greenish grey and dark brown samples were collected at ~2 km from the Mémel site, nearby Pouth – kélle area.

Two grey and light grey samples were collected from Nsime – Kélle area (~10 km from the Pouth – kélle area). One dark orange and one

Table 1
Macroscopic description of talc schist samples and their localizations.

Localities	Samples	GPS coordinates	Elevation (m)	Colours
Mémel	WE1	N03°52′22.8′′; E011°30′21.1″	210 ± 3	10YR5/3, Greyish olive
	WE2			10YR4/5, Reddish brown
	WE3			10YR5/4, Olive
	WE4	N03°48′12.0′′; E010°46′30.6″	217 ± 3	10YR5/3, Greyish olive
	WE5, WE6, WE7	N03°48′10.8′′; E010°46′29.4″	211 ± 3	10YR5/1, Grey
	WE8			10YR5/4, Yellowish brown
	WE9			10YR6/4, Light yellowish brown
	WE10			10YR5/1, Grey
	WE11	N03°48′10.1′′; E010°46′28.8″	211 ± 3	10YR5/1, Grey
	WE12	N03°48′09.8′′; E010°46′28.9″	214 ± 3	10YR6/1, Brownish grey
	WE13			10YR6/5, Bright yellowish brown
	WE14			10YR6/3, Olive yellow
	WE15	N03°48′08.7′′; E010°46′27.0″	215 ± 3	10YR5/1, Grey
	WE16, WE17	N03°49′34.3′′; E010°47′17.2″	236 ± 3	10YR5/1, Grey
	WE18, WE19, WE20	N03°49′34.1′′; E010°47′16.7″	229 ± 3	10YR5/1, Grey
	WE21, WE22, WE23, WE26, WE27, WE28	N03°49′33.8′′; E010°47′16.8″	225 ± 3	10YR4/1, Dark greenish grey
	WE29, WE30, WE31	N03°49′33.5′′; E01047′17.5″	223 ± 3	10YR6/1, Light grey
	WE32, WE33, WE34, WE35	N03°49′07.6′′; E010°47′58.4″	223 ± 3	10YR6/6, Yellowish brown
Pouth- kéllé	WE36, WE37, WE38, WE39	N03°49′46.8′′; E010°48′3.9″	219 ± 3	10YR6/1, Greenish grey
	WE40, WE41	N03°49′50.1′′; E010°48′30.5″	230 ± 3	10YR5/3, Dull brown
Nsimé -kéllé	WE42	N04°00′16.6′′; E011°03′12.8″	390 ± 3	10YR5/1, Grey
	WE43			10YR6/2, Light grey
Maholo	WE44	N04°00′06.8′′; E011°03′09.9″	400 ± 3	10YR7/5, Dull orange
Manguenda -hegba	WE45	N03°58″44.7′′; E011°02′43.2″	435 ± 3	10YR8/4, Light orange

light orange sample were sampled from Maholè and Manguenda – Hegba areas, respectively.

3.2. Analytical methods

Talc schist samples were characterized texturally (grain-size), mineralogically (XRD), chemically (XRF), petrographically (thin sections), and thermally (DTA/TG).

Grain-size distribution of the talc schist samples was perfomed using a laser diffraction particle size analyzer Malvern Mastersizer 2000 at the University of Liège (Belgium).

X-ray diffraction (XRD) of bulk sediments was performed on all collected samples, using a Bruker diffractometer with CuKα radiation (Department of Geology, University of Liège). The angular range explored was between 5° and 60° 2θ. The bulk sample was dried in an oven at 25 °C and then ground to <250 μm. The X-ray patterns were processed using the DIFFRACT PLUS EVA software, and mineralogical composition were quantified by the Rietveld Method using Topas v5 software (Bruker).

Additional measurements were carried out on oriented aggregates prepared from the < 2 μm fraction (Moore and Reynolds, 1989). Clay mineralogy <2 μm fraction was carried out from the suspension according to Stoke's law, placed on a glass slide and the XRD patterns recorded between 2° and 30° 2 theta using the same step size and time per step parameters mentioned before. These oriented aggregates were subjected to three successive treatments, air drying (N), glycolation (EG) and heating to 500 °C for 4 h. Semi-quantitative estimations (±5–10%) were based on the height of a diagnostic peak multiplied by a correction factor and the mineral abundances are normalized to 100% (Biscaye, 1965; Boski et al., 1998). The common reflection of clays at 4.47 Å is multiplied by a corrective factor of 20 to give an estimate of the total clays in the bulk sample.

Chemical composition of major and minor elements was carried out by X-Ray Fluorescence spectroscopy, using a portable X-ray fluorescence spectrometer (*p*-XRF) Thermo Fischer Nitron XL3t with a 'GOLDD' detector (Mineralogy Laboratory, University of Liege). The *p*-XRF was placed against the gem or glass bead and X-rays were generated when the nosecone was in direct contact with the surface. The X-ray spot size was 3 mm in diameter. The X-ray tube has an Ag anode of 50 kV and 200 μA. The lightest detectable element is Mg. The standardization mode selected is the ''Cu/Zn Mining'' mode, which includes all elements. This mode uses four separate filters to determine the concentrations in percentage of elements: a high filter (15s counting time), a main filter (15s) a low filter (15s), and a light filter (30s), leading to a total measurement time of 75s per analysis. The software utilizes a Fundamental Parameters algorithm to determine concentrations of each element. The spectra and concentration values obtained from the XLT3 were downloaded to a computer for analysis. Each sample was measured three times.

Thin sections were performed on tow representative samples; the richest (WE16) and the least rich (WE44) in talc. Weathered samples of talc schist were consolidated by impregnation with an epoxy resin and then polished. The thin sections were studied using a polarizing light microscope.

The physico-chemical changes in terms of increased temperature were determined using differential thermal (DTA) analysis coupled with thermogravimetry (TG) on samples representative of the chemical and mineralogical variations in the different sites. This analysis was performed on nine samples (i.e WE45, WE43, WE42, WE40, WE39, WE37, WE34, WE16 and WE2). The ATD/TG analysis was carried out using a TGA-2000 Analyzer type that allows TGA-2000 automatic multi-gravimetric thermogravimetric analysis under atmospheric conditions (Department of Geology, University of Liège). The sample was heated from room temperature to 1000 °C at a rate of 5 °C/min. In this work, differential thermal analysis is coupled with thermogravimetry. The results obtained allow to determine the degree of hydration as well as the decomposition temperatures of the various components.

Scanning Electronic Microscope (SEM) images were obtained on a talc rich sample (WE29) by using a Philips microscope model XL30 (University of Aachen, Germany). In situ chemical composition was determined by Energy Dispersive X-ray spectroscopy (EDX). The images were obtained with a secondary electron detector at a voltage of 10 kV on gold-sputtered powdered samples.

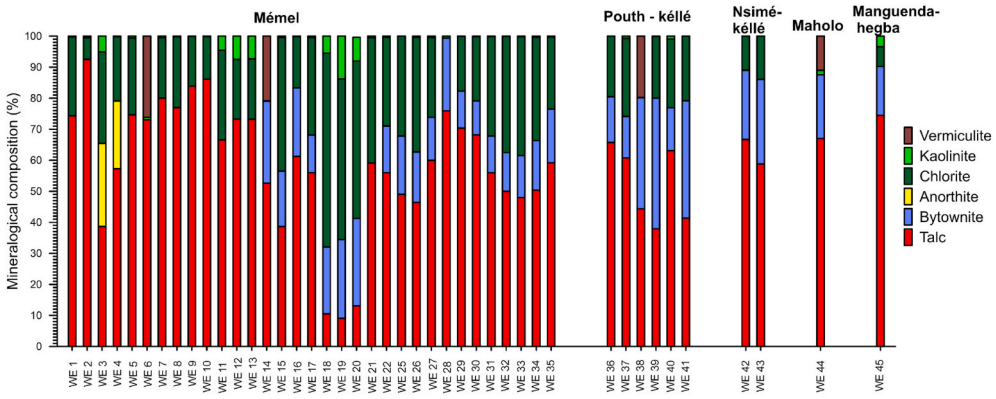

Fig. 3. Mineralogical composition of talc schist samples.

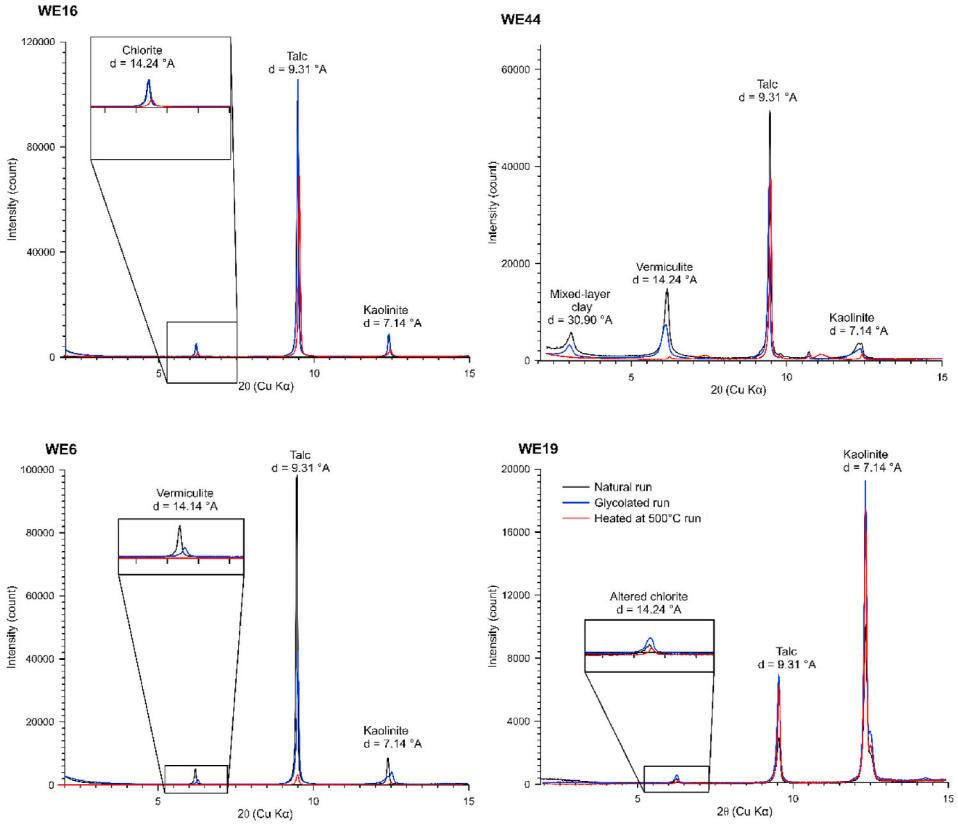

Fig. 4. Spectra of clay mineral (<2 μm). WE16, WE6 and WE19 at Memel; WE45 at Manguenda – hegba.

4. Results

4.1. Mineralogical composition

4.1.1. Bulk fraction

Mineralogical composition of the talc schist samples shows large variability. Talc represents the major phase and is associated with plagioclase and clay minerals (Fig. 3).

At Memél, the samples are mainly composed of talc (58 ± 20%), chlorite (29 ± 29%), plagioclase phases (25 ± 4%) and traces of clay phases; kaolinite (2 ± 3%) and vermiculite. At Pouth – kéllé, talc (49 ± 12%) is associated with chlorite (22 ± 2%), variable amounts of plagioclase (29 ± 14%) and sporadically trace of vermiculite (WE38). At Nsimé – kéllé, talc (63 ± 6%) is the major phase associated with plagioclase (25 ± 4%) and small amounts of chlorite (12 ± 2). At Maholè and Manguenda – Hegba areas, talc remains the major phase (71 ± 5%) associated with the occurrence of plagioclase (18 ± 3%) and small amounts of clay phases; chlorite (9 ± 3%) and kaolinite (2 ± 1%). Traces of amphibole (~2%) occur only in samples WE44.

4.1.2. Clay fraction (<2 μm)

XRD spectra of clay fractions (<2 μm) show the occurrence of talc, kaolinite, chlorite and vermiculite (Fig. 4). Talc appears at d = 9.31 Å which remains unchanged after ethylene glycol solvation and heating at 500 °C. Chlorite shows characteristic peaks at d = 14.24 Å and d = 7.14 Å, the latter peak is also due to the contribution of kaolinite. XRD spectra reveal mainly altered chlorite (Fig. 4). The detrital chlorite shows variation in basal reflections in different samples indicating that different Fe content of the chlorite.

Kaolinite seems to be authigenic, since it was not possible to separate a 3.57 A reflection for kaolinite from the 004 chlorite reflection at 3.54 A indicating the absence of detrital kaolinite. Kaolinite mainly occurs in

Table 2
Major and minor chemical composition (wt.%) of the talc schist samples. Three replicate measurements were carried out for each samples and an average and standard deviation value is reported.

Localities	Samples	SiO_2 (%)		MgO (%)		Fe_2O_3 (%)		Al_2O_3 (%)		TiO_2 (%)		Cr (%)		Ni (%)		Zn (%)	
Mémel	WE1	57.51	±0.28	13.33	±0.68	21.73	±0.11	7.31	±0.14	0.12	±0.01	0.47	±0.01	0.29	±0.01	0.02	±0.003
	WE2	56.60	±0.23	9.47	±0.48	25.39	±0.10	8.33	±0.11	0.21	±0.01	0.32	±0.01	0.20	±0.01	0.01	±0.002
	WE3	56.08	±0.21	13.52	±0.49	21.90	±0.08	8.40	±0.10	0.11	±0.01	0.30	±0.01	0.18	±0.01	0.01	±0.002
	WE4	61.24	±0.32	18.35	±0.87	15.91	±0.10	4.42	±0.14	0.07	±0.01	0.23	±0.01	0.41	±0.02	0.02	±0.003
	WE5	55.20	±0.25	15.21	±0.65	18.13	±0.09	11.43	±0.15	0.04	±0.01	0.36	±0.01	0.31	±0.01	0.02	±0.002
	WE6	55.48	±0.27	16.39	±0.74	17.58	±0.09	10.47	±0.17	0.08	±0.01	0.35	±0.01	0.33	±0.01	0.01	±0.002
	WE7	62.22	±0.25	16.29	±0.62	14.13	±0.07	7.31	±0.12	0.05	±0.00	0.20	±0.01	0.33	±0.01	0.01	±0.002
	WE8	62.72	±0.22	15.26	±0.50	14.90	±0.06	7.01	±0.10	0.09	±0.00	0.20	±0.01	0.28	±0.01	0.01	±0.002
	WE9	62.91	±0.24	15.80	±0.57	15.08	±0.07	6.17	±0.10	0.04	±0.00	0.24	±0.01	0.32	±0.01	0.01	±0.002
	WE10	63.39	±0.24	16.74	±0.58	13.98	±0.06	5.86	±0.10	0.03	±0.00	0.22	±0.01	0.30	±0.01	0.01	±0.002
	WE11	54.76	±0.22	9.44	±0.47	26.59	±0.09	9.14	±0.11	0.07	±0.00	0.42	±0.01	0.12	±0.01	0.01	±0.003
	WE12	49.71	±0.22	14.22	±0.62	24.13	±0.10	11.88	±0.15	0.06	±0.01	0.65	±0.01	0.20	±0.01	0.01	±0.002
	WE13	47.21	±0.23	13.57	±0.65	26.97	±0.13	12.13	±0.16	0.12	±0.01	0.67	±0.01	0.26	±0.01	0.01	±0.002
	WE14	60.90	±0.28	16.72	±0.71	16.11	±0.08	6.24	±0.13	0.03	±0.01	0.28	±0.01	0.24	±0.01	0.02	±0.003
	WE15	54.46	±0.27	20.29	±0.77	14.50	±0.08	10.71	±0.16	0.04	±0.01	0.08	±0.00	0.34	±0.01	0.01	±0.002
	WE16	60.02	±0.23	20.17	±0.63	17.52	±0.07	2.26	±0.08	0.04	±0.00	0.15	±0.00	0.25	±0.01	0.01	±0.002
	WE17	55.50	±0.22	18.96	±0.62	21.12	±0.08	4.32	±0.09	0.09	±0.01	0.30	±0.01	0.32	±0.01	0.01	±0.002
	WE18	55.37	±0.21	21.63	±0.63	19.05	±0.07	3.89	±0.09	0.06	±0.00	0.34	±0.01	0.21	±0.01	0.01	±0.002
	WE19	52.18	±0.19	22.87	±0.60	19.79	±0.07	5.09	±0.09	0.07	±0.00	0.22	±0.01	0.24	±0.01	0.01	±0.002
	WE20	57.52	±0.26	17.91	±0.71	18.73	±0.09	5.54	±0.12	0.30	±0.01	0.21	±0.01	0.29	±0.01	0.01	±0.002
	WE21	56.17	±0.24	21.37	±0.70	13.90	±0.07	8.48	±0.13	0.07	±0.01	0.45	±0.01	0.28	±0.01	0.01	±0.002
	WE22	52.27	±0.25	23.16	±0.84	19.91	±0.10	4.62	±0.12	0.05	±0.01	0.53	±0.01	0.26	±0.01	0.01	±0.002
	WE25	53.37	±0.29	18.76	±0.86	18.28	±0.11	9.56	±0.18	0.02	±0.01	0.51	±0.01	0.35	±0.02	0.03	±0.003
	WE26	54.63	±0.22	17.19	±0.60	18.91	±0.08	9.21	±0.12	0.06	±0.01	0.45	±0.01	0.23	±0.01	0.02	±0.002
	WE27	55.32	±0.23	18.46	±0.64	21.49	±0.09	4.70	±0.10	0.03	±0.00	0.40	±0.01	0.23	±0.01	0.01	±0.002
	WE28	51.90	±0.20	15.57	±0.52	20.88	±0.07	11.52	±0.11	0.13	±0.01	0.24	±0.01	0.21	±0.01	0.01	±0.002
	WE29	65.09	±0.21	18.54	±0.49	11.00	±0.05	5.18	±0.08	0.20	±0.01	0.04	±0.00	0.21	±0.01	0.01	±0.001
	WE30	58.41	±0.24	16.70	±0.57	15.85	±0.07	8.99	±0.12	0.04	±0.00	0.36	±0.01	0.25	±0.01	0.01	±0.002
	WE31	56.06	±0.25	21.18	±0.74	17.39	±0.08	5.33	±0.12	0.04	±0.00	0.33	±0.01	0.28	±0.01	0.01	±0.002
	WE32	49.78	±0.19	15.68	±0.52	20.88	±0.07	13.56	±0.13	0.10	±0.01	0.34	±0.01	0.24	±0.01	0.01	±0.002
	WE33	47.21	±0.21	17.41	±0.61	20.34	±0.08	15.00	±0.16	0.04	±0.01	0.39	±0.01	0.26	±0.01	0.01	±0.002
	WE34	49.44	±0.23	19.35	±0.70	18.15	±0.09	12.91	±0.16	0.15	±0.01	0.30	±0.01	0.28	±0.01	0.01	±0.002
	WE35	51.82	±0.23	15.84	±0.66	25.17	±0.11	7.13	±0.12	0.04	±0.01	0.30	±0.01	0.28	±0.01	0.01	±0.002
Pouth - kéllé	WE36	56.00	±0.25	20.32	±0.76	20.15	±0.10	3.47	±0.11	0.06	±0.01	0.56	±0.01	0.30	±0.01	0.02	±0.002
	WE37	51.20	±0.28	19.89	±0.90	22.10	±0.13	6.72	±0.16	0.08	±0.01	0.85	±0.01	0.34	±0.02	0.02	±0.003
	WE38	60.44	±0.13	19.31	±0.44	15.93	±0.04	4.28	±0.07	0.04	±0.00	0.54	±0.01	0.25	±0.01	0.02	±0.001
	WE39	64.34	±0.19	16.60	±0.43	16.53	±0.05	2.50	±0.06	0.03	±0.00	0.18	±0.00	0.14	±0.01	0.01	±0.002
	WE40	54.65	±0.24	18.59	±0.70	20.42	±0.09	6.32	±0.12	0.03	±0.01	0.66	±0.01	0.24	±0.01	0.02	±0.003
	WE41	63.34	±0.23	18.37	±0.58	15.58	±0.06	2.69	±0.08	0.03	±0.00	0.17	±0.00	0.17	±0.01	0.01	±0.002
Nsimé - kéllé	WE42	62.99	±0.27	19.18	±0.71	15.11	±0.08	2.68	±0.10	0.03	±0.00	0.24	±0.01	0.25	±0.01	0.01	±0.002
	WE43	65.15	±0.24	17.37	±0.56	15.15	±0.07	2.31	±0.08	0.02	±0.00	0.18	±0.01	0.18	±0.01	0.01	±0.002
Maholo	WE44	54.57	±0.23	18.04	±0.68	23.87	±0.10	3.49	±0.10	0.03	±0.01	0.20	±0.01	0.17	±0.01	0.02	±0.002
Manguenda- hegba	WE45	86.03	±0.33	7.72	±0.46	3.65	±0.04	2.59	±0.10	0.00	±0.01	0.14	±0.01	0.06	±0.01	<LOD	±0.003

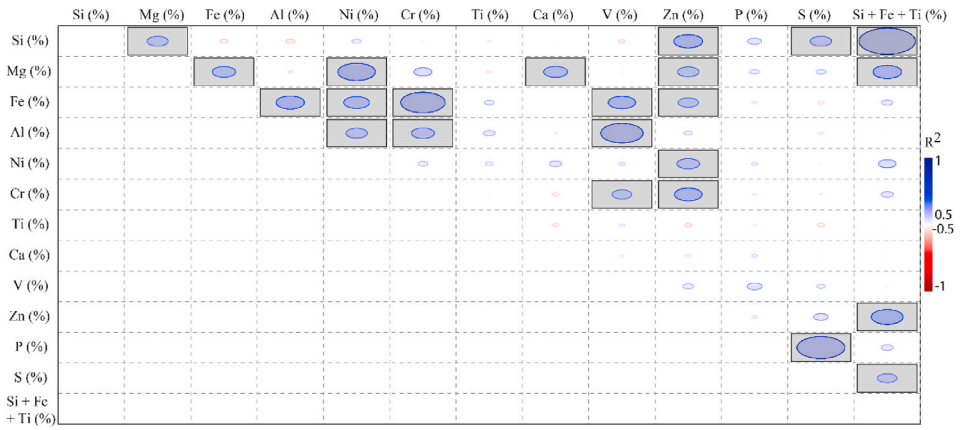

Fig. 5. Spearman's rank correlation matrix for talcshist samples based on XRF data, considering a correlation significant, if $R^2 > 0.50$.

small amount, in association with chlorite in some samples from most of the sites studied. Vermiculite shows a peak at d = 14.14 Å in natural and after ethylene glycol saturation, which shifts towards d = 10 Å after heating at 500 °C (Fig. 4). Vermiculite occurs locally alone or in association with kaolinite in Memel, Maholè and Pouth – Kéllé areas.

Mixed-layer chlorite/vermiculite (corrensite) occurs only in WE44 sample from Maholè area. It is characterized by a basal spacing of 29 Å, which expands to 31 Å after ethylene glycol treatment and collapses to 24 Å after heating at 500 °C (Fig. 4). Corrensite is associated with vermiculite and traces of kaolinite, plagioclase and talc.

4.2. Chemical composition

Talc schist samples from the Mémel site are rich in silica (25.7 ± 4.1%), the lowest content (14.1%) is found in sample WE11 and the highest (34.7%) in sample WE4. Variable amounts of magnesium (10.3 ± 2.3%) and iron (6.5 ± 1.5%) compose these samples, the lowest values are 3.1% (WE11) and 3.2% (WE29) and the highest ones are 15.4% and 10.6% for WE22 and WE13, respectively. Aluminum (2.09 ± 1%) is also present in small amounts. Low percentages (<1%) of Ca, Ti, V, Cr, Ni, Zn, P and S are present (Table 2).

The Pouth - Kelle site has the same chemical composition as the Mémel site, with a slight increase in silica content (28.2 ± 3.8%). The highest Si percentage is found in sample WE38 (31.5%) and the lowest in sample WE39 (20.9%). Magnesium content (12.1 ± 3.1%) is slightly higher that the Mémel site, with the lowest value of 6.7% (WE39) and the highest one of 15.5% (WE36). Likewise, iron values (9 ± 2.1%) show similar variations to the Mémel site. The contents of the other elements are very low (Table 2).

The Nsime- Kellé site is composed of variable amounts of silica (29.9 ± 4.2%) and magnesium (11.1 ± 2.6%). Lower values of iron (5.3 ± 0.9%) than the Pouth - kelle and Mémel sites compose these samples. The contents of other elements are very low (<1%).

For the Maholè and Manguenda- Hegba sites, high variability in chemical composition is observed (Table 2 XRF). The contents are higher in silica (37.7 ± 14.7%). Magnesium contents (8.6 ± 4.3%) range from 5.6% (WE45) to 11.7% (WE44). Likewise, iron shows an important variability from 1.5% (WE44) to 8.95% (WE44).

Spearman's rank correlation analysis performed on the data sets enabled the identification of possible common characteristics (e.g. origin, weathering, behaviour) of major and traces elements in talc schist samples. The correlation matrices obtained for talc schist samples, display two groups of associations: one for Cr, V and S (R2 = ~0.9), and another for Ni, Mg, Al, Ca and Zn (R2 = 0.5–0.6) (Fig. 5https://www.sciencedirect.com/science/article/pii/S0045653507000148?casa_token=mWRyHDEbBeMAAAAA:e9tG83LvT2T1PlRpjlNu-mLIiXBtEuxaxFrsU8wtyB30Nnkb0-26FuChnyUr7HUfh36zaSEf40M - tbl3). For the first group, Cr, V and S have a strong positive correlation with Fe, Al and P. The second group has a moderate positive correlation with Si and Cr.

Three main observations can be drawn from the above: (i) Si + Fe + Ti displays good positive correlation with Si; (ii) Fe is highly correlated with Cr and V; (iii) S has a good correlation with P. This implies ultramafic origin of talc rich samples and the occurrence of hydrothermal fluid circulation.

4.3. Petrography, grain-size and morphology

On thin sections the talc schist samples have an appearance similar to micas (Fig. 6 a, a'). They are foliated, and appear in the form of aggregates and fibers, with opaque inclusions. They are non-pleochroic, with fibers having a positive elongation. Clay appears as matrix associated with talc fibers. Light grey clay is also observed in the shape of balls, suggesting its possible secondary origin (Fig. 6 c, c').

Tremolite appears as pale green to grey elongated fibers with opaque inclusions in natural light (Fig. 6 b, b', c, c'). The extinction angles are variable, characterized by a positive elongation. Most of opaque inclusions are surrounded by talc fibers, with a yellowish to mauve color in natural light, which becomes light green in polarized light. Traces of cleavage and a weak to moderate pleochroism are quite visible.

Fig. 7 indicates a homogeneous grain-size for the talc schist samples with a mean grain-size (D50) comprised between 30 and 87 μm, the samples are classified as silty sand or sandy silt.

SEM images of sample WE29 (Fig. 8) indicate that talc particles have lamellar shape with some irregularity at the boundaries. The lamellar morphology allows particle stacking and weak packing cohesion leading to partial exfoliation. EDX spectrum shows that the selected grain contain Al, Si and O which are dominant associated with variable quantities of Mg, K, and Ca and a low quantities of Fe and Na.

4.4. Thermal behavior of talcschist

The DTA thermograms (Fig. 9) of the samples studied display two

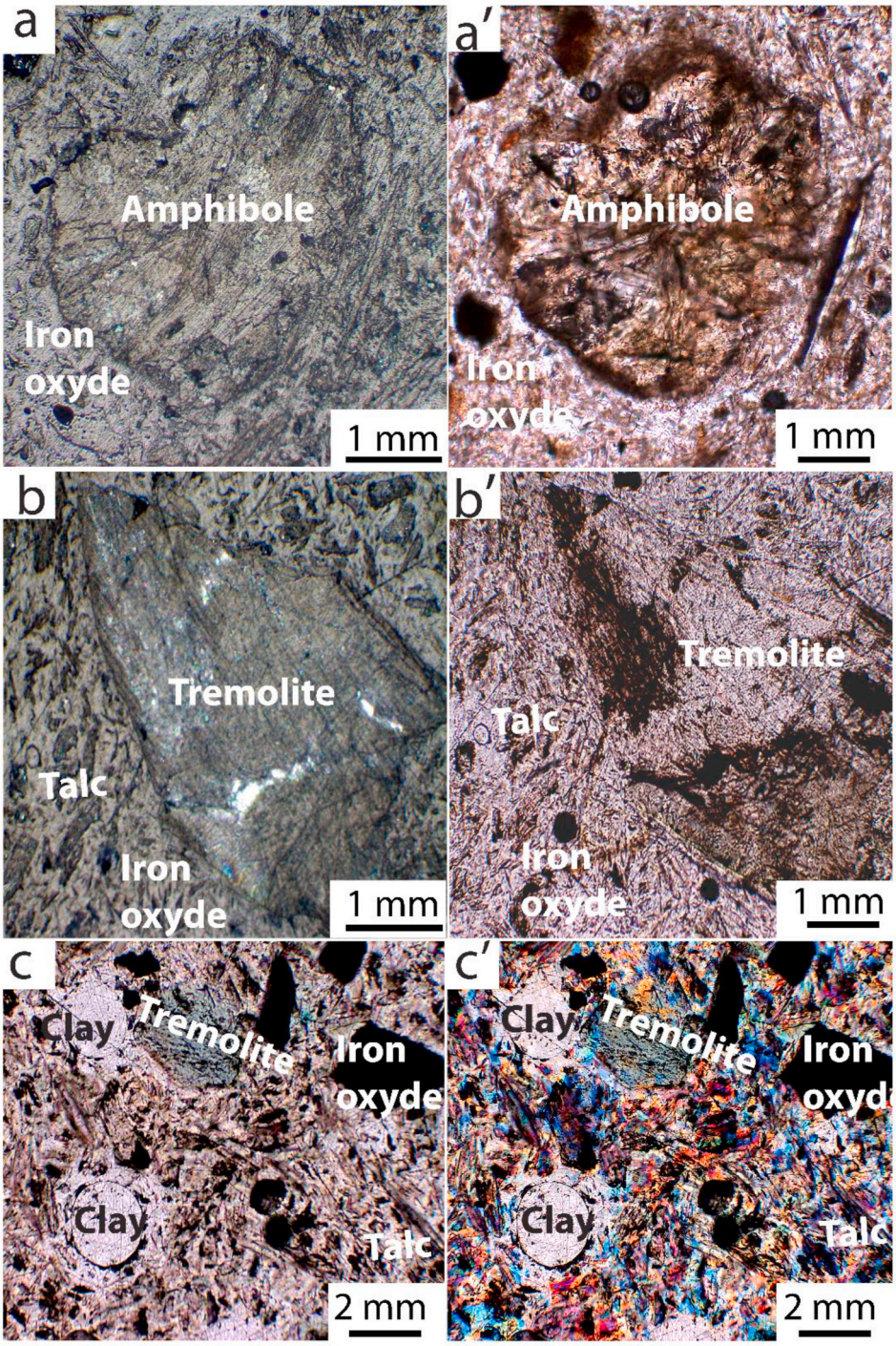

Fig. 6. Photomicrographs of polished thin sections of talc schist samples in natural (a, b, c) and (a', b', c') polarized light. a. amphibole surrounded by iron oxides and talc fibers (WE44) from Pouth-kéllé; b. elongated tremolite surrounded by talc fibers (WE44) from Pouth –kéllé; c. talc fibers associated with matrix of clay (WE16) at Mémel.

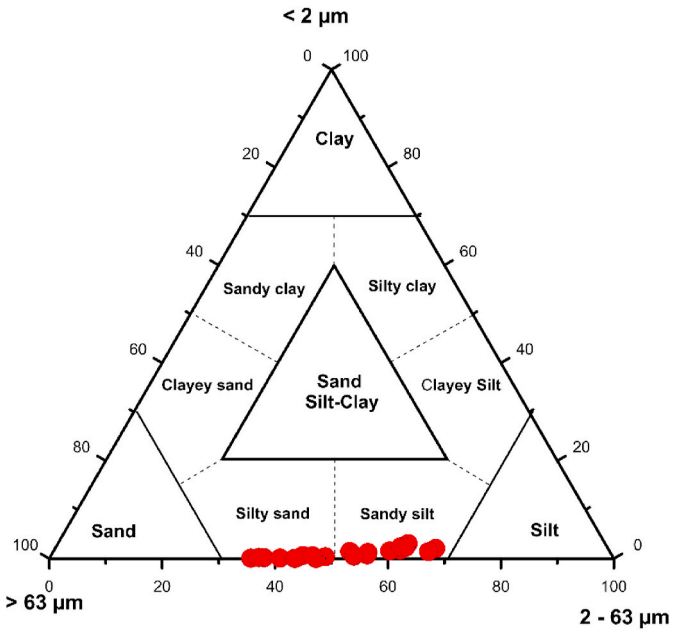

Fig. 7. Grain size distribution of the talc schist samples.

endothermic events between ~500 °C and ~600 °C peaks, associated with a loss of mass. The first peak at 500 °C corresponds to the dehydroxylation of kaolinite (WE2) and the peaks at ~600 °C represents chlorite dehydroxylation (WE34). All the samples display an endothermic peak between 900 °C and 1000 °C associated with a loss of mass. This peak corresponds to the dehydroxylation of talc ($Si_4Mg_3O_{10}$ (OH)$_2$). Talc is transformed into clinoenstatite (MgO, SiO_2) following the equation below (Grosjean, 1984):

$$4SiO2\ 3MgO,\ H2O\ (talc) \rightarrow 3MgO.SiO2\ (clinoenstatite) + SiO2\ (cristobalite) + H2O\ (1)$$

5. Discussion

5.1. Talc schist characterization

Mineralogical composition of the talc schist samples shows a large variability, in agreement with previous studies in the Boumnyebel area (Nkoumbou et al., 2006a, 2006b). Talc occurs as a major phase associated with plagioclase and clay minerals (Fig. 3). Talc is associated with chlorite and goethite in the Lamal Pougue area in Cameroon (Nkoumbou et al., 2006a), and with chlorite, actinolite and calcite in the Ermidag deposit in Turkey (Ersoy et al., 2013). However, major chemical composition is homogenous and mainly consist of Si, Mg and Fe as shown in Fig. 10(Fig. 10) (Petit et al., 2004). As an exception sample WE45 from Manguenda –Hegba has the highest amount of silica, reflecting the signature of possible ultramafic parent rock. The chemical composition is in line with previous studies in Cameroon (Nkoumbou et al., 2006a). The occurrence of variable amounts of magnesium, iron, chromium and nickel (Table 2) implies features of ultramafic protoliths (Nkoumbou et al., 2006a, b). They contrast with the Trimouns deposit, which formed from the alterationof dolomitic carbonate rocks situated in tectonic contact with metamorphic siliceous rocks (Marteau et al., 1991).

Based on the ternary diagrams (Fig. 10), there is no obvious correlation between chemical and mineralogical distribution of talc schist samples and the talc amount in the localities studied (Fig. 10). A three clusters are deciphered based on the occurrence of clay mineral phases and plagioclase in talc schist samples regardless of the sampling location: (i) talc rich samples with small amount of plagioclase, (ii) talc rich samples without plagioclase, (iii) the poorest talc samples (0–40%) with high amounts of clay minerals mainly chlorite and very small amounts (<5%) of plagioclase.

Thermal analysis of talc schist samples display endothermic peaks between 450 and 600 °C due to the occurrence of chlorite (Fig. 9). Similar endothermic peaks were reported in talc schist from Cameroun (Nkoumbou et al., 2006a) and Turkey (Ersoy et al., 2013). The latter observed that endothermic peaks disappeared with increasing talc contents in the samples. The talc studied shows a large endothermic peak between 900 °C and 1000 °C, corresponding to dehydroxylation of talc which is transformed into clinoenstatite. Whereas, in Nkoumbou et al. (2006a), dehydroxylation of talc occurred between 850 and

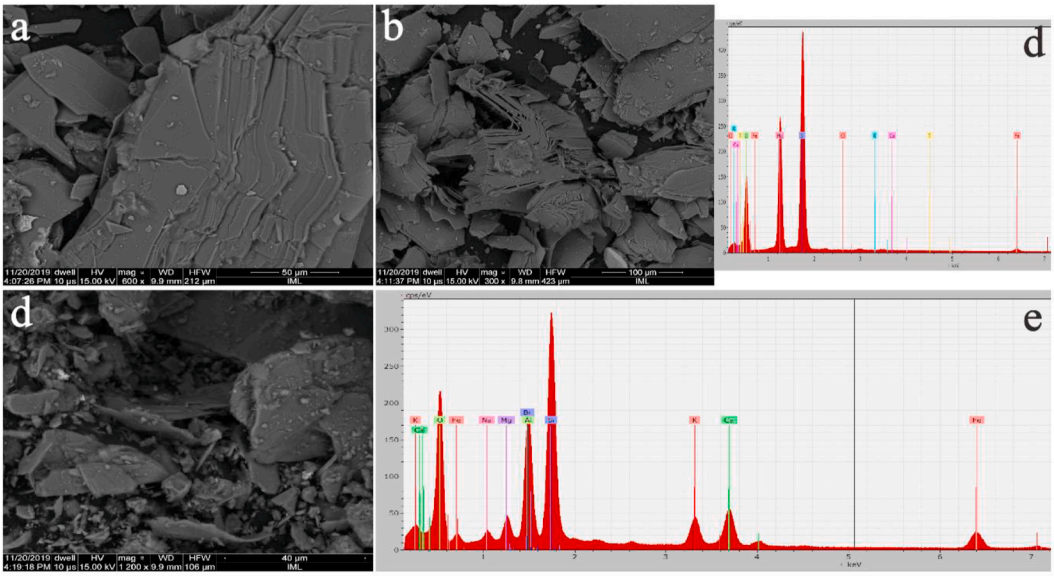

Fig. 8. SEM images and EDX results obtained from sample WE29. a–b: talc; d: EDX of talc; d: plagioclase. d–e: EDX results.

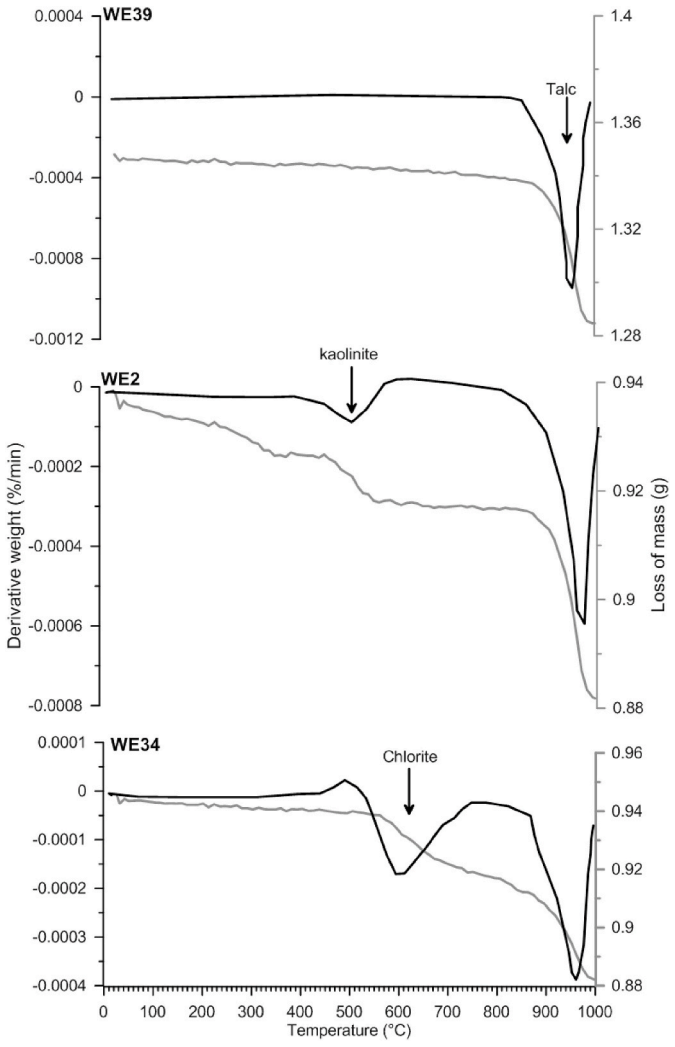

Fig. 9. Thermogravimetric diagrams of the talc schist samples from Pouth –kéllé (WE39) and Mémel (WE2 and WE34).

1050 °C leading to tremolite formation.

Talc has a platy morphology as shown in SEM images (Fig. 9). Similar morphology of talc were reported in talcschists from Cameroon (Nkoumbou et al., 2006a, 2008a; Ngally Sabouang 2014). Talc ore from the province of Cordoba in Argentina which formed in meta-ultramafic rocks, has planar crystals forming packets of superimposed sheets (Lescano et al., 2017).

5.2. Source and weathering trend

Ferromagnesian, corrensite and chlorite are widespread products of hydrothermally-altered mafic rocks (Abad et al., 2003). In hydrothermal systems, the circulation of a hot hydrothermal fluid causes the crystallization of chlorite and corrensite in the more distal area, this alteration of the bedrock might have begun even during the contact metamorphism stage.

In the studied area, mineral characterization and the XRD spectra of the clay fraction (Fig. 4) reveal that vermiculite; kaolinite and talc are the dominant secondary minerals formed during weathering (Righi and Meunier, 1995). These three secondary minerals can be used as indicators to determine the regional weathering degree. Concerning the origin of vermiculite, two major hypotheses have been considered: vermiculization of biotite, and alteration of pyroxene and hornblende. Previous studies pointed out that vermiculization of biotite results from a replacement of interlayer K by hydrated cations generally Mg resulting in structural changes from trioctahedral to dioctahedral, and eventually oxidation of structural Fe (e.g. Churchman and Lowe, 2012; Feng et al., 2018; Kudrashou et al., 2020; Moore and Reynolds, 1989). The alteration of biotite to vermiculite is caused by the superficial circulation of groundwater, which leached potassium from biotite and then from vermiculite (Narasimha et al., 2006). Alteration of pyroxene and hornblende into vermiculite has also been reported in mafic and ultramafic rocks due to the fluid infiltration during acidic intrusion (e.g. Fanning et al., 1989; Narasimha et al., 2006).

Kaolinite may be formed from two sources: either neoformation from feldspar; or alteration of vermiculite. Neoformation of kaolinite from alteration of feldspar is the most common weathering process in humid tropical regions such as North Eastern Cameroon. It acts specifically in moderately drained and weakly acid environments with low silica activity (Churchman et al., 2010). The opposite variation of kaolinite (0–40%) and vermiculite (0–20%) suggests that kaolinite may be derived from the transformation of vermiculite by losing Mg and Si (Sanjurjo et al., 2001).

Weathering in the region studied is also confirmed by the geochemical composition of major elements with selective accumulation of iron-rich minerals as indicated by the Al/Fe ratio below 1. Si, Al and Fe are positively correlated with most of the traces elements (Ni, V, Zn, Cr), suggesting their possible incorporation in newly formed clay minerals, especially vermiculite.

According to Nkoumbou et al. (2006a), most of the trace elements are compatible with tremolite formed by hydrothermal transformation of ultramafic rocks. Based on the high talc contents of the rocks and occasional coexistance of tremolite and magnesio-riebeckite, the origin of the talc sediment is assigned to a hydrothermal alteration of ultramafic rocks (Nkoumbou et al., 2008a). The occurrence of high contents of Cr and Ni indicate genetic relation with ultramafic rocks (Table 2). The hydrothermal origin is also supported by the occurrence of P and S, and their high correlation with silica (Angerer et al., 2013) (Fig. 5).

6. Conclusion

Talc schist deposits from central Cameroon region have been characterized. Different alteration zones in talc schist deposits were determined depending on differences related to the texture and color of the host rocks.

Mineralogical composition of talc schist samples is variable and shows the occurrence of talc as major phase associated with variable contents of plagioclase and clay minerals. Three groups of mineral parageneses were determined: i) talc with small amount of chlorite and traces of kaolinite, ii) talc with high amount of chlorite, iii) variable amount of talc with plagioclase and clay minerals.

Talc schist samples showed strong correlation between Cr, V and S (R2 = ~0.9) and Fe is highly correlated with Cr and V. This implies an ultramafic origin of the talc schist and the occurrence of hydrothermal fluid circulation.

Talc particles have lamellar shapes with some irregularity at the boundaries. The lamellar morphology allows particle stacking and weak packing cohesion leading to partial exfoliation. Talc chemistry mainly

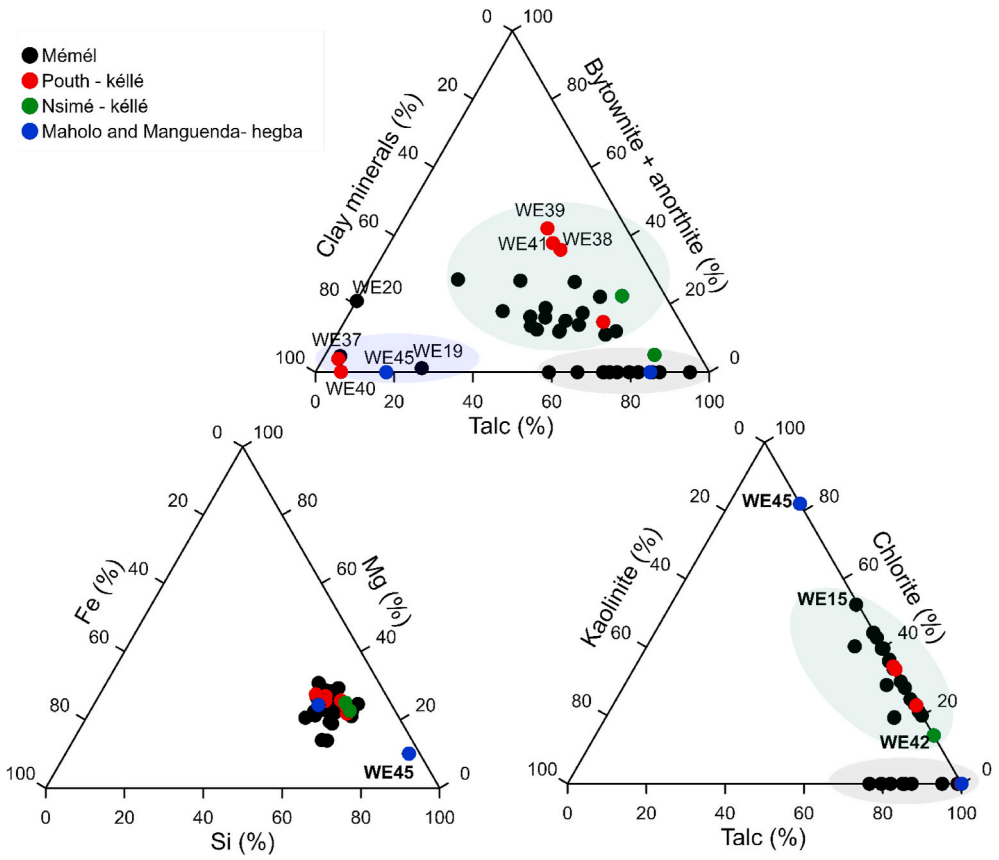

Fig. 10. Ternary diagrams with end members of Fe/Mg/Si and kaolinite/chlorite/talc.

consist of Al, Si and O with variable quantities of Mg, K, and Ca and low quantities of Fe and Na.

The characteristics obtained of the clay fraction associated with talc suggests that these talc schist samples could potentially be a source of ceramic raw material.

Declaration of competing interest

The authors declare that they have no known competing financial interests or personal relationships that could have appeared to influence the work reported in this paper.

Acknowledgements

The Author greatly appreciate the financial help of research program for development ARES – CCD for the field work, the author thanks Mr Metang (University of Yaoundé I, Cameroon) for the support during field work.

References

Abad, I., Jiménez-Millán, J., Molina, J.M., Nieto, F., Vera, J.A., 2003. Anomalous reverse zoning of saponite and corrensite caused by contact metamorphism and hydrothermal alteration of marly rocks associated with subvolcanic bodies. Clay Clay Miner. 51 (5), 543–554.

Akpanika, O.I., Ukpong, E.E., Olade, M.A., 1987. Mineralogy and geochemical dispersion in tropical residual soils overlying a talc deposit in southwestern Nigeria. Chem. Geol. 63 (1–2), 109–119.

Ali-Bik, M.W., Taman, Z., El Kalioubi, B., Wahab, W.A., 2012. Serpentinite-hosted talc–magnesite deposits of Wadi Barramiya area, Eastern Desert, Egypt: characteristics, petrogenesis and evolution. J. Afr. Earth Sci. 64, 77–89.

Angerer, T., Kerrich, R., Hagemann, S.G., 2013. Geochemistry of a komatiitic, boninitic, and tholeiitic basalt association in the Mesoarchean Koolyanobbing greenstone belt, Southern Cross Domain, Yilgarn craton: implications for mantle sources and geodynamic setting of banded iron formation. Precambrian Res. 224, 110–128.

Biscaye, P.E., 1965. Mineralogy and sedimentation of recent deep-sea clay in the Atlantic Ocean and adjacent seas and oceans. Geol. Soc. Am. Bull. 76, 803–832.

Boski, T., Pessoa, J., Pedro, P., Thorez, J., Dias, J.M.A., Hall, I.R., 1998. Factors governing abundance of hydrolyzable amino acids in the sediments from the NW European Continental Margin (47–50° N). Prog. Oceanogr. 42, 145–164.

Churchman, G.J., Lowe, D.J., 2012. Alteration, Formation, and Occurrence of Minerals in Soils. CRC press, pp. 1–72.

Davison, I., Dos Santos, R.A., 1989. Tectonic evolution of the Sergipano fold belt, NE Brazil, during the Brasiliano orogeny. Precambrian Res. 45 (4), 319–342.

Dumas, A., Martin, F., Le Roux, C., Micoud, P., Petit, S., Ferrage, E., Brendlé, J., Grauby, O., Greenhill-Hooper, M., 2013. Phyllosilicates synthesis: a way of accessing edges contributions in NMR and FTIR spectroscopies. Example of synthetic talc. Phys. Chem. Miner. 40 (4), 361–373.

Ersoy, B., Dikmen, S., Yildiz, A., Goren, R., Elitolk, O., 2013. Mineralogical and physicochemical properties of talc from Ermidag, Afyonkaralisar, Turkey. Turk. J. Earth Sci. 632–644, 10.3906/yer -1112-14.

Evans, B.W., Guggenheim, S., 1988. Talc, pyrophyllite, and related minerals. In: Hydrous Phyllosilicates (Exclusive of Micas) (SW Bailey, Editor), vol. 19. Reviews in Mineralogy, p. 225À294.

Fanning, D.S., Keramidas, V.Z., El-Desoky, M.A., 1989. In'Minerals in Soil Environments, 2nd Edn.(Eds. Soil Sci. Soc. Am, Madison, pp. 551–634.

Feng, B., Song, D., Fu, L., Jiang, Z., Yuan, Y., 2018. Formation Principles of Calcification Precipitation and Hydrothermal Alteration Minerals in Guide Basin Gringha. American geophysical union.

Gil, G., Gunia, P., Barnes, J.D., Szymański, M., Jokubauskas, P., Kalbarczyk-Gil, A., Bagiński, B., 2020. Origin of talc and Fe-Ti-V mineralization in the Kletno deposit (the Śnieżnik Massif, SW Poland). Minerals 10 (1), 13.

Grosjean, P., 1984. Contribution à la monocuisson rapide de faïence au talc. Etude de pâtes et émaux. In: Application à l'industrie du carreau de revêtement (suite), 780. L'Industrie céramique, Paris, pp. 106–114.

Kudrashou, V.Y., Nasr El Din, H.A., 2020. Formation damage associated with mineral alteration and formation of swelling clays caused by steam injection in sand packs. SPE Reservoir Eval. Eng. 23, 326–344. https://doi.org/10.2118/195700-PA, 01.

Laplaine, L., 1969. Indices minéraux et ressources minérales du Cameroun. Bulletin de la direction des mines et de la géologie 5.

Lescano, L., Locati, F., Sfragulla, J., Marfil, S., Bonalumi, A., Maiza, P., 2017. Asbestiform and non-asbestiform morphologies in a talc and vermiculite mine from the province of Córdoba (Argentina): a case study. Environ. Earth Sci. 76 (18), 1–20.

Marteau, P., Grès, M., Guillaneau, J.C., 1991. Memento roches et minéraux industriels Talc. BRGM. Service Géologique National.

Metang, V., Nkoumbou, C., Tchakounté, N.J., Njopwouo, D., 2014. Application of remote sensing for the mapping of geologicalstructures in mainforest area: acase study at the

Matomb – Makak area, Center – south Cameroon. Journal of Geosciences and Geomatics 2 (5), 196–207. https://doi.org/10.12691/jgg-2-5-3.
Moore, D.M., Reynolds, R.C., 1989. X-ray Diffraction and the Identification and Analysis of Clay Minerals, vol. 322. Oxford University press, Oxford.
Narasimha, K.N.P., Ramalingaiah, H., Melka, K., Krishnaveni, K., Prasad, P.S., Krishnaiah, C., Jayappa, K.S., Ganesha, A.V., 2006. Vermiculite mineralization associated with ultramafics in Agasthyapura area, Mysore dist., Karnataka state, India-A mineralogical study. Acta Geodyn. Geomater. 3 (4), 19.
Nédélec, A., Macaudière, J., Nzenti, J.P., Barbey, P., 1986. Evolution structurale et métamorphique des schistes de Mbalmayo (Cameroun). Implications pour la structure de la zone mobile pan-africaine d'Afrique centrale, au contact du craton du Congo. Comptes rendus de l'Académie des sciences. Série 2, Mécanique, Physique, Chimie, Sciences de l'univers, Sciences de la Terre 303 (1), 75–80.
Ngally S, C.J., Mbey, J.A., Liboum, Thomas, F., Njopwouo, D., 2014. Talc as raw material for cementitious products formulation. Journal of Asian ceramic society 2 (3), 263–267.
Nkoumbou, C., Njopwouo, D., Villieras, F., Njoya, A., Yonta, N.C., Ngo Njock, L., Tchoua, F.M., Yvon, J., 2006a. Talc indices from Boumnyebel (Central Cameroon), physico-chemical characteristics and geochemistry. J. Afr. Earth Sci. 45 (1), 61–73.
Nkoumbou, C., Villieras, F., Njopwouo, D., Yonta, N.C., Barres, O., Pelletier, M., Razafitianamaharavo, A., Yvon, J., 2008a. Physicochemical properties of talc ore from three deposits of Lamal Pougué area (Yaoundé Pan-African Belt, Cameroon), in relation to industrial uses. Appl. Clay Sci. 41 (3–4), 113–132.
Nkoumbou, C., Villieras, F., Njopwouo, D., Yonta, N.C., Barres, O., Pelletier, M., Razafitianamaharavo, A., Yvon, J., 2008b. Physicochemical properties of talc ore from Pouth- kélle and Mémel deposits (Central Cameroon). Clay Miner. 43 (2), 317–337.
Nkoumbou, C., Yonta, Ngouné, C., Villieras, F., Njopwouo, D., Yvon, J., Ekodeck, G.E., Tchoua, F.M., 2006b. Découverte de roches à affinité ophiolitiques dans la chaine panafricaine au Cameroun : talcschistes de Ngoung, Lamal Pouguè et Bibodi Lamal. Compt. Rendus Geosci. 338 (16), 1167–1175.
Ntep, G.P., 2001. Ressources minérales du Cameroun- Notice explicative de la carte thématique des ressources minérales du Cameroun sur fond géologique. Sopecam, Yaoundé, p. 375.
Nzenti, J.P., Barbey, P., Macaudiere, J., Soba, D., 1988. Origin and evolution of late Precambrian high-grade Yaoundé gneisses. Precambrian Res. 38 (2), 91–109.
Owona, S., Schulz, B., Ratschbacher, L., Ondoa, J.M., Ekodeck, G.E., Tchoua, F.M., Affaton, P., 2011. Pan-African metamorphic evolution in the southern Yaounde Group (Oubanguide Complex, Cameroon) as revealed by EMP-monazite dating and thermobarometry of garnet metapelites. J. Afr. Earth Sci. 59 (1), 125–139.
Petit, S., Martin, F., Wiewora, A., DE Parseval, P., Decarreau, A., 2004. Crystal chemistry of talc: a near infrared (NIR) spectroscopy study. Am. Mineral. 89 (2–3), 319–326.
Pouclet, A., Vidal, M., Doumnang, J.C., Vicat, J.P., Tchameni, R., 2006. Neoproterozoic crustal evolution in southern Chad: Pan –African ocean basin closing, arc accretion and late – to – post orogenic granitic intrusion. J. Afr. Earth Sci. 44 (4–5), 543–560.
Prochaska, W., Mogessie, A., Raith, J.G., 1992. Formation of the talc deposit of Kibanda (Rwanda) and its relation to the regional metamorphic evolution. J. Afr. Earth Sci. 14 (4), 499–509.
Righi, D., Meunier, A., 1995. Origin of clays by rock weathering and soil formation. In: Origin and mineralogy of clays. Springer, Berlin, Heidelberg, pp. 43–161.
Sanjurjo, M.J.F., Corti, G., Ugolini, F.C., 2001. Chemical and mineralogical changes in a polygenetic soil of Galicia, NW Spain. Catena 43 (3), 251–265.
Schandl, E.S., Gorton, M.P., Sharara, N.A., 2002. The origin of major talc deposits in the Eastern Desert of Egypt: relict fragments of a metamorphosed carbonate horizon? J. Afr. Earth Sci. 34 (3–4), 259–273.
Stendal, H., Toteu, S.F., Frei, R., Penaye, J., Njel, U.O., Bassahak, J., Kankeu, B., Ngako, V., Hell, J.V., 2006. Derivation of detrital rutile in the Yaounde region from the Neoproterozoic Pan-African belt in southern Cameroon (Central Africa). Journal of African Earth Sciences 44 (4–5), 443–458.
Tosca, N.J., Macdonald, F.A., Strauss, J.V., Johnston, D.T., Knoll, A.H., 2011. Sedimentary talc in Neoproterozoic carbonate successions. Earth Planet Sci. Lett. 306 (1–2), 11–22.
Yonta, N.C., 2010. Le contexte géologique des indices de talc de la région de boumnyebel (chaine panafricaine d'Afrique central-Cameroun). In: PhD thesis in Geology, université de Yaoundé I, Cameroun and université Henri Poincaré. Nancy, France.
Yonta-Ngoune, C., Nkoumbou, C., Barbey, P., Le Breton, N., Montel, J.M., Villiéras, F., 2010. Geological context of the Boumnyebel talcschists (Cameroun): inferences on the Pan-African Belt of Central Africa. Comptes Rendus Géoscience 342 (2), 108–115.